Predicting Early-Age Fracture Pattern of UHPC Cylinders Using Categorical Performance Density Diagrams

Micah Stark – (corresponding author) Graduate Assistant Researcher, Texas A&M University, Zachry Department of Civil and Environmental Engineering, College Station, TX, USA, Email: mdstark@tamu.edu

Cesario Tavares, PhD – Postdoctoral Researcher, Texas A&M University, Zachry Department of Civil and Environmental Engineering, College Station, TX, USA, Email: cesariotavares@tamu.edu

Pratik Gujar, PhD – Postdoctoral Researcher, Texas State University, Ingram School of Engineering, San Marcos, TX, USA, Email: mle99@txstate.edu

Xijun Shi, PhD, PE – Assistant Professor, Texas State University, Ingram School of Engineering, San Marcos, TX, USA, Email: xijun.shi@txstate.edu

Kinsey Skillen, PhD – Assistant Professor, Texas A&M University, Zachry Department of Civil and Environmental Engineering, College Station, TX, USA, Email: skillen@tamu.edu

Abstract

Fracture pattern of concrete cylinders tested under uniaxial compression has been associated with many different factors. Literature suggests that saturation level, mix constituents, fiber content, curing temperature and specimen end conditions can play a crucial role in failure mode. As such, tools capable of modeling fracture pattern as a function of mix composition and curing conditions are attractive to help understand microstructural behavior. In particular, understanding the relationship between binder matrices and fiber reinforcement in dictating crack propagation could facilitate the development of ultra-high-performance concretes (UHPC) with enhanced ductility. In this study, orthogonal arrays are coupled with a k-nearest neighbors' model to reduce the experimental runs needed to predict fracture patterns (following ASTM C39/C39M) of UHPC cylinders tested for compressive strength at age 24 hours. Processed data shows strong correlation between fracture type, mix constituents and compressive strength. Therefore, mix proportions with different contents of slag, microsilica and fly ash were used as model features, along with their respective compressive strengths. The model was trained on 85% of the experimental data while validation was performed in the remaining 15%. A 79% model accuracy was obtained using a k-fold cross validation process, suggesting that this method is suitable to estimate behavior in small datasets. The predictions obtained are illustrated through categorical and probabilistic performance density diagrams to facilitate the evaluation of the synergistic relationship between raw constituents and fracture pattern. This method could be used in future work to improve the ductility and cost-efficiency of UHPC through optimization of fiber content.

Keywords: Fracture Pattern, UHPC, Machine Learning, Mixture Design

Publication type: Full Paper
Paper No: 102

1. Introduction

The fracture pattern observed in concrete cylinders when tested under uniaxial compression is a function of many factors. Saturation level, microstructural properties, curing conditions, fiber reinforcement, and specimen-end conditions all play their part in determining where and how cracks initiate and propagate through a specimen.

The effects of water saturation on strength characteristics and failure behavior of cement mortars subjected to static and dynamic compressive loading has been investigated by Mustafa et al. (12). The experimental observations indicate that saturated mortar samples under static loading exhibited lower compressive strengths but increased ductility when compared to the dry samples. Additionally, saturated samples under dynamic loading showed higher impact resistance and fracture toughness with fracture propagation to smaller depths when compared to the dry samples.

Aggregate type and fiber contents have also been reported to affect fracture pattern. Siringi et al. (223-26) studied the use of crumb rubber as a partial replacement of fine aggregates and reported that concrete mixtures with crumb rubber exhibited a ductile failure under compressive loading without excessive cracking running through the length of the specimen. In contrast, mixtures with conventional fine aggregates exhibited a brittle failure, with cracks running through the specimen. Meanwhile, Gacu and Sim (1496-97) studied the effects of adding marble microparticles on the physical and mechanical properties of concrete. Cone and split type fractures were observed when no microparticles were added. On the other hand, cone type fracture was observed for mixtures with 2.5% and 5% microparticles. Xu et al. (783-84) tested the unconfined compressive strength of fiber reinforced cement tailings backfill with different percentages of polypropylene (PP) fibers. Columnar tensile failures were observed in samples with no fibers cured at 20°C and 35°C, while hybrid failure was observed in samples cured at 50°C. On the other hand, a shear type failure was observed with the addition of fibers. Tayebi and Nematzadeh (16) also observed diagonal (shear) failure with fiber reinforced samples when testing the effect of hot compacted waste nylon fiber on the compressive stress-strain behavior of steel fiber reinforced concrete after exposure to fire. Similarly, Shi et al. (5-6) observed shear failure with increases in fiber content and noted a new bulging type failure in PP fiber reinforced concrete.

Literature also suggests that specimen end conditions influence the failure pattern observed in concrete cylinders. Roddenberry et al. (86) studied the failure behavior of concrete cylinders under different end conditions. Following the definitions from ASTM C39/C39M (6), Roddenberry reported that cylinders with high surface friction failed in Type 1 or 2 modes (cone or cone/column hybrid modes), whereas cylinders with reduced surface friction failed in Type 3 mode (columnar mode, where cracks run the complete length of the cylinder parallel to the applied compressive load). It is suggested that the friction between the specimen surface and the bearing plates and the amount of confinement controls the fracture pattern in concrete cylinders. Koh et al. (192) also observed distinctive failure locations for capped and non-capped specimens made of calcium sulfate dihydrate cements when testing them under unconfined, uniaxial compression.

These observations suggest that fracture pattern could provide insight into microstructural behavior affecting performance. Thus, a tool capable of modeling fracture pattern as a function of mix constituents and curing conditions is of great interest to researchers and material engineers developing innovative concrete formulations. In particular, for Ultra-High-Performance Concretes (UHPC) and Fiber Reinforced Concretes (FRC), such tool could foster the development of highly ductile materials through a synergistic optimization of the binder matrix and fiber reinforcement.

In this study, a methodology proposed in (Tavares et al. 5) (combining orthogonal arrays and machine learning) is used to effectively estimate fracture pattern as a function of mix proportioning while performing a reduced number of experimental runs. UHPC binders with varying replacement levels of slag, microsilica and fly ash were produced and tested under uniaxial compression. Failure types were recorded as shown in Figure 1 following ASTM C39/C39M-21 (6). Predictions obtained from the models are further displayed using categorical and probabilistic performance density diagrams (PDD) to facilitate the interpretation of the trends observed in the domain and enable an intuitive estimation of the fracture pattern for different mix compositions.

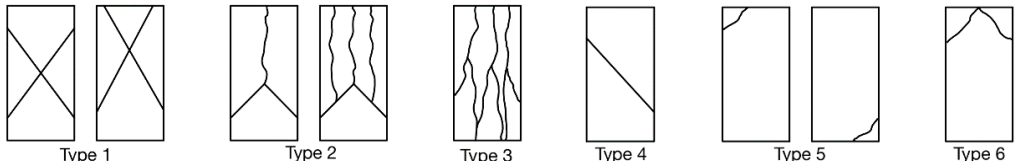

Figure 1: ASTM C39/C39M Fracture Types (adapted from (ASTM_C39/C39M-21 6))

2. Materials and Methods

Orthogonal arrays from the Taguchi method were used to collect strategic data points within the domain of interest to train a k-nearest neighbors'(knn) model that estimates fracture pattern as a function of mix proportions. The content of supplementary cementitious materials (SCMs) was defined in the basis of a percentage by weight (wt.) replacing ordinary portland cement (OPC) in the matrix. The maximum contents of slag, microsilica and fly ash were fixed at 60%, 20% and 15%, respectively, following the reasoning detailed in (Tavares et al. 4). The experimental framework used for data collection was designed using an L25 orthogonal array with slag, microsilica and fly ash contents as the variables. The water-to-cementitious ratio (w/cm) and high-range water reducer content (HRWR/cm) were initially fixed at 0.2 and 1%, respectively. Adjustments in the HRWR content were made as needed, targeting flow values between 25-40 cm. This was done to account for the incorporation of aggregates later in that study (Tavares et al. 3), thus ensuring that the flow values of the final UHPC mortars would stand within the thresholds specified by ASTM C1856/1856M (1) (20-25cm). To fit the data with the knn model, the adjusted values of w/cm and SCM replacement levels were used as the model variables/features to predict compressive strengths. Finally, a categorical knn model for fracture pattern was developed using compressive strength and the three SCM replacement levels as the features/variables. Reasoning behind feature selection in each stage is detailed in (S.G.M. e Tavares 50-67).

Motivated by the resource and time-consuming nature of typical standard methods, this study was performed using a novel test protocol that facilitates extensive data collection to feed machine learning models. This protocol consists of an expedited production process involving 0.9 x 1.8 in (23 x 46 mm) cylinders, cast in silicone molds as shown in Figure 2 a), allowing large datasets to be generated in short periods of time. These specimens consume approximately forty times less material by volume compared to the 3-by-6 in cylinders used in ASTM C1856/1856M, while the casting time is approximately seven times faster. Both ends of the cylinders were cut prior to testing to obtain the aforementioned dimensions while the capping method consisted of placing commercially available felt cushion pads at the ends of the cylinders during testing.

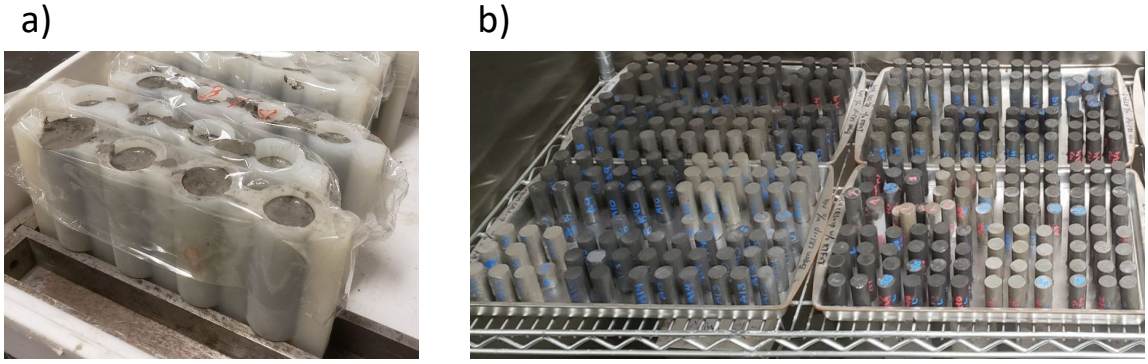

Figure 2: a) Silicone molds used to cast UHPC binders in this; b) specimens curing at 23°C and RH 100%

As shown in (Tavares et al. 11), this protocol emulates results obtained following ASTM C1856/1856M for binders and mortars with compressive strengths up to 120 MPa. Figure 2b) illustrates specimens cast during the mixing phase, curing at 23°C and RH 100%.

3. Results and Discussion

Data from UHPC binders tested at age 24 hours during Phase A in (Tavares et al. 9) were used to develop the model herein. Compressive strengths and fracture types were recorded as shown in Table 1.

Table 1. Experimental Results – adapted from (S.G.M. e Tavares 46)

Mixture #	SCM replacing cement (% by wt.)			w/cm	HRWR/cm	flow (cm)	testing at age 1 day		
	Slag	Microsilica	Fly Ash				avg fc (MPa)	sd (MPa)	Fracture Type
A1	0	0	0	0.19	1.2%	26	63.3	2.4	3,3,3
A2	0	5	3.75	0.20	1.7%	31	79.6	3.6	3,3,3
A3	0	10	7.5	0.20	2.3%	31.5	71.2	1.7	3,3,2
A4	0	15	11.25	0.20	2.9%	28.5	36.9	3.7	3,3,2
A5	0	20	15	0.21	3.4%	25	25.7	3.0	3,3,1
A6	15	0	3.75	0.19	1.4%	36.5	56.9	4.8	3,3,3
A7	15	5	7.5	0.20	1.7%	36	45.1	3.3	3,3,3
A8	15	10	11.25	0.20	2.3%	34	32.1	3.4	3,3,3
A9	15	15	15	0.20	2.9%	31	22.8	2.4	3,3,3
A10	15	20	0	0.21	3.5%	25	35.1	1.7	3,3,3
A11	30	0	7.5	0.19	1.3%	38	43.8	11.8	3,3,3
A12	30	5	11.25	0.19	1.4%	37	36.7	6.9	3,3,3
A13	30	10	15	0.20	2.0%	35	29.3	2.6	2,2,3
A14	30	15	0	0.21	3.3%	30.5	24.4	1.4	1,2,3
A15	30	20	3.75	0.21	3.7%	26	12.6	0.3	1,1,1
A16	45	0	11.25	0.19	1.0%	35	28.2	3.5	2,2,2
A17	45	5	15	0.19	1.3%	36.5	30.1	1.0	2,2,2
A18	45	10	0	0.20	2.0%	33	33.7	1.7	2,2,3
A19	45	15	3.75	0.20	2.3%	31	20.6	0.8	2,2,2
A20	45	20	7.5	0.22	5.1%	31	2.5	0.3	1,1,1
A21	60	0	15	0.20	1.6%	38	8.7	0.1	1,1,1
A22	60	5	0	0.19	1.4%	32.5	32.0	1.8	2,2,3
A23	60	10	3.75	0.19	1.5%	29.5	21.5	0.5	2,2,3
A24	60	15	7.5	0.21	4.0%	33	4.3	0.4	1,1,1
A25	60	20	11.25	0.21	3.3%	29	4.7	0.9	1,1,1

Mixture# - mix design number; avg fc - average compressive strength (MPa); sd - standard deviation (MPa); 6.895 MPa = 1 ksi

For each mixture design, the average compressive strength (in MPa), standard deviation (in MPa), measured spread flow (in cm) and fracture type observed for three specimens are presented. A strong correlation was observed between the fracture type and the compressive strength during data processing. Thus, in addition to the SCM variables, the compressive strengths were also used to predict the fracture type. First, different kNN models were evaluated in predicting the compressive strength at age 24 hours as a function of the SCM replacement levels and w/cm. Details of this model development can be found in (S.G.M. e Tavares 50-67). The best performing compressive strength model in (S.G.M. e Tavares 65) was used to generate a vector with predicted compressive strengths for all the possible mix combinations within the domain of interest. Next, a categorical kNN model was built using slag, microsilica, fly ash and predicted compressive strength as the features, while training the model on 85% of the data. Figure 3 illustrates the k-fold cross validation process used to optimize the tuning parameter "k" for this classification model.

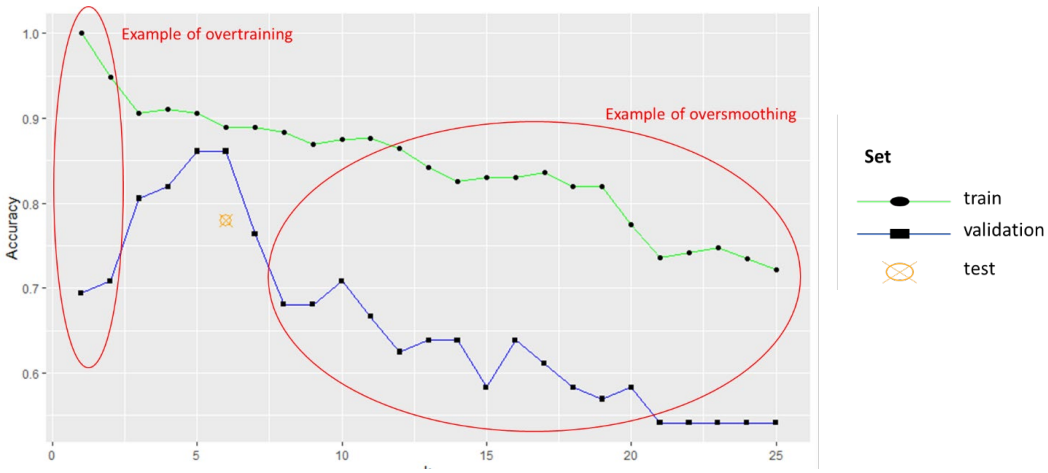

Figure 3. Tuning parameter optimization for the kNN model. The maximum average accuracy in the validation sets was obtained with k=6. After defining the kNN model with k=6, k-fold cross validation was performed in a similar manner, creating different test set folds to estimate the overall model accuracy.

For categorical outcomes, the goal consists of maximizing the average accuracy across the validation sets in each k-fold (15% of the data in each fold). As it can be observed, the optimum k parameter was found to be equal to 6, where a balanced accuracy across the training and validation sets were observed, at 88% and 86%, respectively. These results indicate that the model was developed without evidence of overtraining and oversmoothing. After defining the optimum "k" value, the model is fit to the unseen data from the testing set to get a better estimate of the accuracy of the model. A 79% accuracy was estimated through the k-fold cross-validation process when fitting the model to the test set. The vector containing the predicted outcomes was combined with the matrix of features to develop a categorical PDD. As defined in (Tavares et al. 8), PDD is a diagram resembling a matrix of contour plots in which the outcome is displayed as the z-coordinate with varying density levels. Figure 4 illustrates the fracture types observed experimentally against the predictions provided by the model through a categorical PDD. It is important to note that, for each mixture design, the fracture type displayed corresponds to the one with higher frequency of occurrence between the three tested specimens.

a)

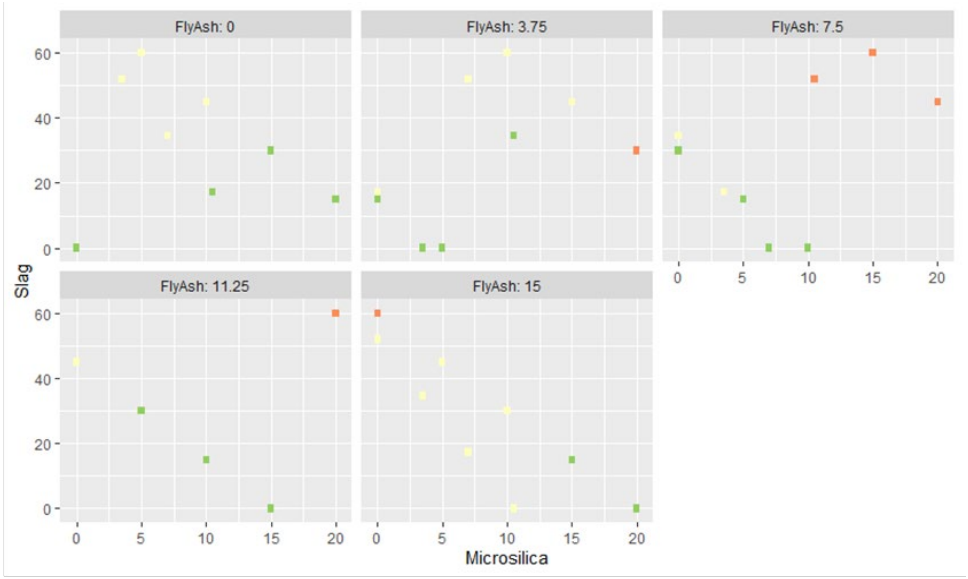

b)

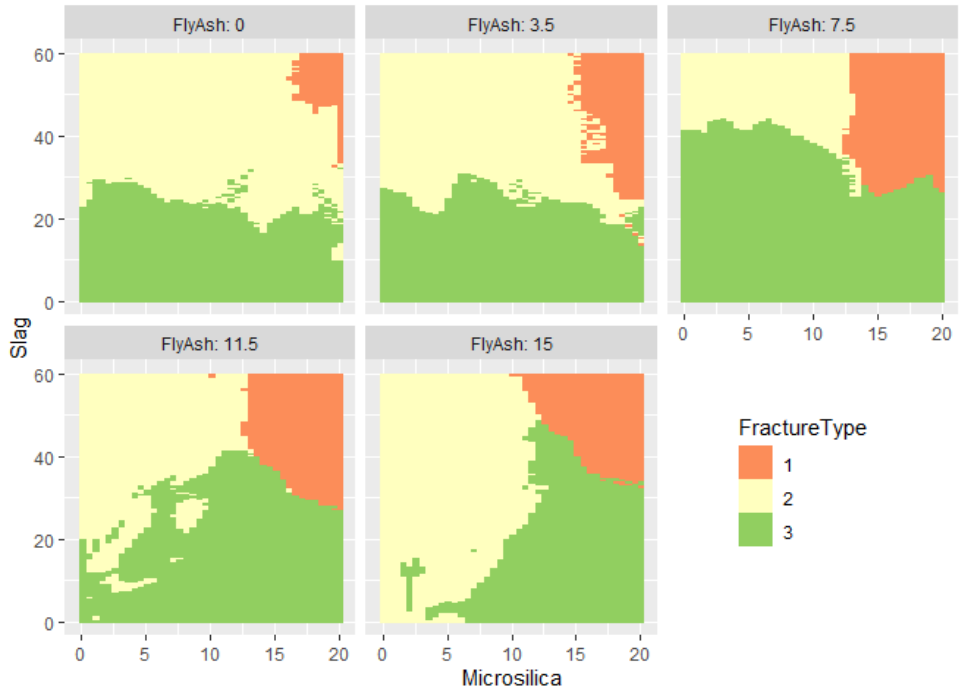

Figure 4: Comparison between experimental results and predictions from categorical PDDs: a) most frequent fracture type observed for each one of the 25 mixtures. Each datapoint defines a mix design with the % by wt. of SCM content replacing cement, while the color describes the fracture type; b) Categorical PDD generated to predict fracture type (S.G.M. e Tavares 76)

For a more conservative evaluation of the observed failure modes, these PDDs can also be built to estimate the probability of occurrence of a given fracture type as a function of changes in mix compositions. A probabilistic PDD is illustrated in Figure 5.

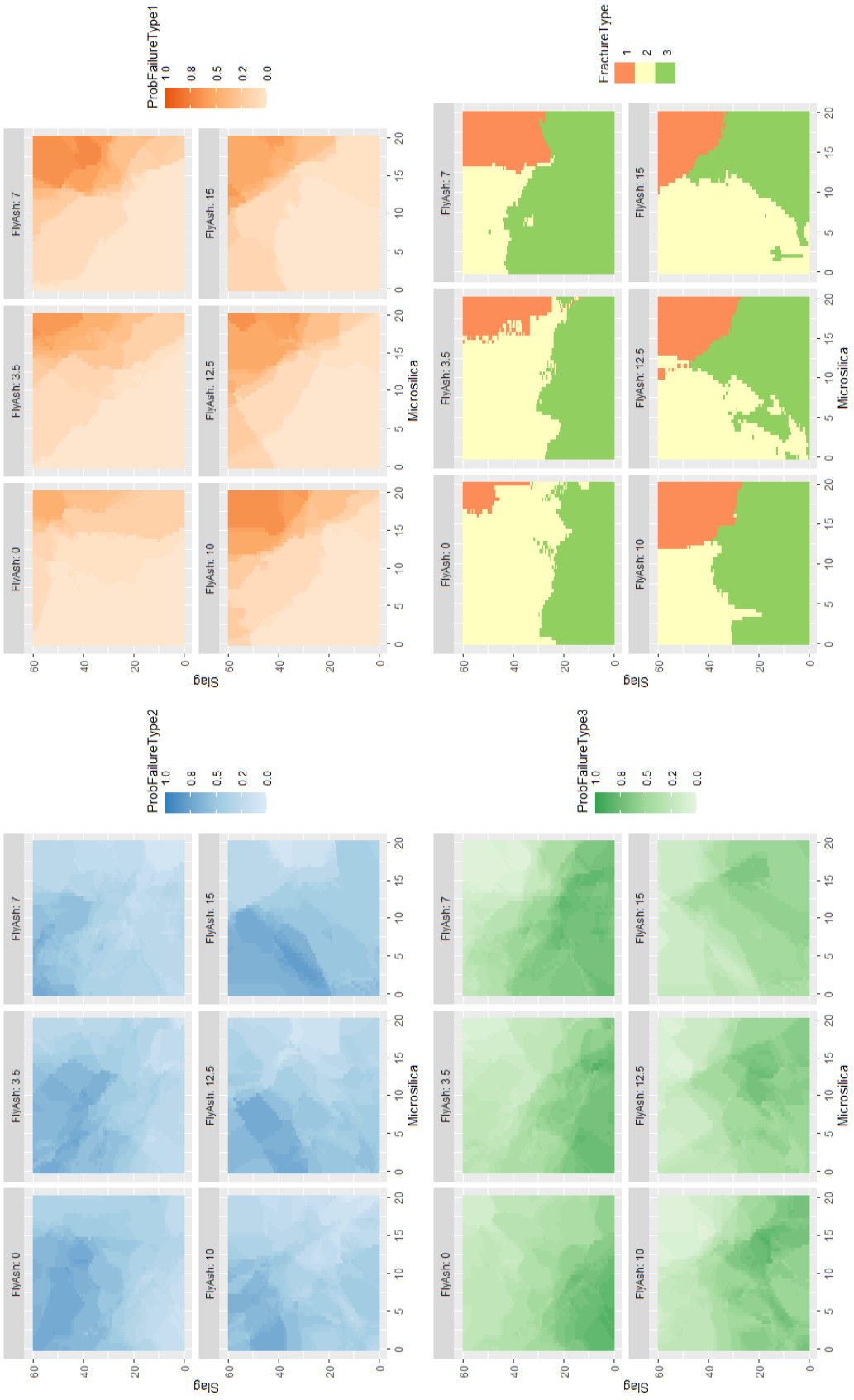

Figure 5: Categorical PDDs generated with a kNN model to predict the fracture type of specimens under uniaxial load as a function of different cement replacement levels of fly ash, slag, and microsilica(S.G.M. e Tavares 77).

As it can be observed, failure modes in Type 1 were mostly associated with high OPC replacement levels with the three SCMs concurrently. This trend makes sense considering that pozzolanic reactions typically occur at later ages, with SCMs not expected to contribute early-age strengths. As expected, materials with less homogeneous microstructures do not tend to exhibit columnar (type 3) failures. Meanwhile, Type 2 was mostly observed for a combination of high slag contents with low microsilica and fly ash contents.

4. Conclusion

In this study, orthogonal arrays were coupled with machine learning models to produce categorical and probabilistic PDDs, developed to facilitate prediction and evaluation of fracture type of UHPC binders as a function of raw ingredients. The models developed effectively predicted fracture type as a function of mix constituents and compressive strengths using a small dataset of cylinders tested under uniaxial compression. This method can be extended to study outcomes such as flexural strains and strengths of UHPC binders with different fiber types and contents. Future work relating different binder systems and associated failure modes with different fiber types (and reinforced at different concentrations) are under investigation. This could ultimately lead to more ductile UHPC compositions, with enhanced flexural capacity and reduced fiber contents, thus contributing to more sustainable and cost-effective concrete infrastructure.

5. References

ASTM_C39/C39M-21. "Standard Test Method for Compressive Strength of Cylindrical Concrete Specimens." West Conshohocken, PA: ASTM International, 2021. Print.

ASTM_C1856/C1856M-17. "Standard Practice for Fabricating and Testing Specimens of Ultra-High Performance Concrete." West Conshohocken, PA: ASTM International, 2017. Print.

Gacu, Jerome G., and Aprille Ann M. Sim. "Effect of Marble Microparticles as Additive on the Physical and Mechanical Properties of Concrete Mixes." *Materials Today: Proceedings* 65 (2022): 1491-97. Print.

Koh, Ilsoo, et al. "The Compressive Modulus and Strength of Saturated Calcium Sulphate Dihydrate Cements: Implications for Testing Standards." *Journal of the Mechanical Behavior of Biomedical Materials* 34 (2014): 187-98. Print.

Mustafa, Ayyaz, et al. "Comparative Analysis of Static and Dynamic Mechanical Behavior for Dry and Saturated Cement Mortar." *Materials* 12.20 (2019). Print.

Roddenberry, M, et al. "Failure Behavior of Concrete Cylinders under Different End Conditions." *ACI Materials Journal* 108.1 (2011). Print.

S.G.M. e Tavares, Cesario. "Multi-Objective Density Diagrams Developed with Machine Learning Models to Optimize Sustainability and Cost-Efficiency of Uhpc Mix Design." Texas A&M University, 2022. Print.

Shi, Feng, et al. "Post-Cracking Behaviour of Basalt and Macro Polypropylene Hybrid Fibre Reinforced Concrete with Different Compressive Strengths." *Construction and Building Materials* 262 (2020): 120108. Print.

Siringi, Gideon M, Ali Abolmaali, and Pranesh B Aswath. "Properties of Concrete with Crumb Rubber Replacing Fine Aggregates (Sand)." *Advances in Civil Engineering Materials* 2.1 (2013): 218-32. Print.

Tavares, Cesario, et al. "Machine Learning-Based Mix Design Tools to Minimize Carbon Footprint and Cost of Uhpc. Part 1: Efficient Data Collection and Modeling." *Cleaner Materials* 4 (2022): 100082. Print.

Tayebi, Morteza, and Mahdi Nematzadeh. "Effect of Hot-Compacted Waste Nylon Fine Aggregate on Compressive Stress-Strain Behavior of Steel Fiber-Reinforced Concrete after Exposure to Fire: Experiments and Optimization." *Construction and Building Materials* 284 (2021): 122742. Print.

Xu, Wenbin, Qianlong Li, and Yalun Zhang. "Influence of Temperature on Compressive Strength, Microstructure Properties and Failure Pattern of Fiber-Reinforced Cemented Tailings Backfill." *Construction and Building Materials* 222 (2019): 776-85. Print.